

pubs.acs.org/JACS Article

Site Densities, Rates, and Mechanism of Stable Ni/UiO-66 Ethylene Oligomerization Catalysts

Benjamin Yeh, Stephen P. Vicchio, Saumil Chheda, Jian Zheng, Julian Schmid, Laura Löbbert, Ricardo Bermejo-Deval, Oliver Y. Gutiérrez, Johannes A. Lercher, Connie C. Lu, Matthew Neurock, Rachel B. Getman, Laura Gagliardi,* and Aditya Bhan*



Cite This: J. Am. Chem. Soc. 2021, 143, 20274-20280



Read Online

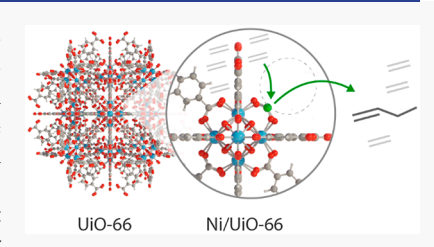
ACCESS

Metrics & More



Supporting Information

ABSTRACT: Nickel-functionalized UiO-66 metal organic frameworks (MOFs) oligomerize ethylene in the absence of cocatalysts or initiators after undergoing ethylene-pressure-dependent transients and maintain stable oligomerization rates for >15 days on stream. Higher ethylene pressures shorten induction periods and engender more active sites for ethylene oligomerization; these sites exhibit invariant selectivity-conversion characteristics to justify that only one type of catalytic center is relevant for oligomerization. The number of active sites is estimated using in situ NO titration to disambiguate the effect of increased reaction rates upon exposure to increasing ethylene pressures. After accounting



for augmented site densities with increasing ethylene pressures, ethylene oligomerization is first order in ethylene pressure from 100 to 1800 kPa with an activation energy of 81 kJ mol⁻¹ at temperatures from 443–503 K on Ni/UiO-66. A representative Ni/UiO-66 cluster model that mimics high ethylene pressure process conditions is validated with ab initio thermodynamic analysis, and the Cossee–Arlman mechanism is posited based on comparisons between experimental and computed activation enthalpies from density functional theory calculations on these cluster models of Ni/UiO-66. The insights gained from experiment and theory help rationalize evolution in structure and stability for ethylene oligomerization Ni/UiO-66 MOF catalysts.

■ INTRODUCTION

Linear alpha olefins (LAOs) comonomers for polyethylene production - 1-butene, 1-hexene, and 1-octene - are produced at 1.1 millon tons a year using a homogeneous nickel catalyst through the Shell Higher Olefin Process (SHOP), which prescribes a Schulz-Flory type distribution for ethylene oligomerization.^{1–3} Nickel-functionalized metal organic frameworks (MOFs)^{4–7} designed with active sites to mimic the catalytic properties of the homogeneous SHOP catalyst⁸ for oligomerization rely on alkyl-aluminum cocatalysts, while nickel-zeolite catalysts viz. Ni/LTA,9 Ni/H-Beta,10 Ni/SSZ-24,¹¹ and Ni/MCM-41,¹² deactivate with time on stream. We report a nickel-functionalized UiO-66 MOF formulation that, after an induction period, exhibits >15 days on-stream stability unprecedented in framework or supported heterogeneous catalytic materials for ethylene oligomerization in the absence of activators and cocatalysts. The Ni/UiO-66 material in this study exhibits first-order kinetics in ethylene pressure after accounting for the on-stream generation of active sites to validate a Cossee–Arlman mechanism^{4–7,9–11} that prescribes physisorbed ethylene in the pores of the MOF framework for ethylene oligomerization. These distinctive characteristics and correspondent mechanisms on Ni/UiO-66 are detailed through transient and steady-state reaction kinetics and density functional theory (DFT) calculations, and the effect of ethylene pressure on rates of reaction is deconvoluted through in situ chemical titration experiments to determine the site

density and reaction order and apparent activation energy for selective 1-butene synthesis.

■ RESULTS AND DISCUSSION

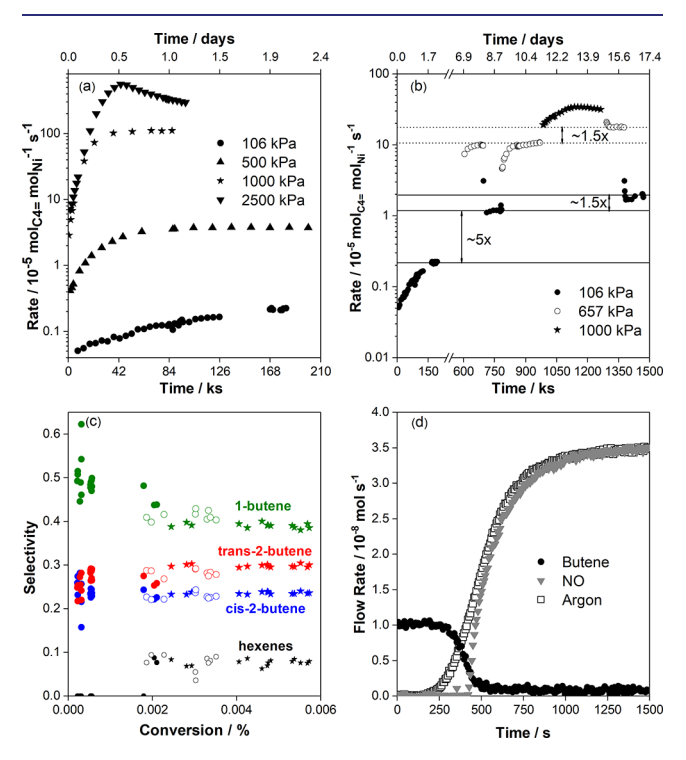
An ideal UiO-66 material has Zr₆O₈ nodes connected with 12 terephthalate ligands. 13-17 Zirconium oxide based MOFs, such as UiO-66 and NU-1000, are characterized with missing linker defects, and single metal atoms and metal-oxide complexes can be anchored on the zirconium-oxide node in lieu of the missing linker defect. $^{18-21}$ We illustrate that nickel species deposited on UiO-66 nodes do not influence the crystallinity, porosity, and thermal stability of the nascent UiO-66 material through powder X-ray diffraction (PXRD), N₂ adsorption, and thermal gravimetric analysis (TGA), respectively; and uniformity of Ni dispersion is evinced by scanning transmission electron microscopy-energy dispersive X-ray spectroscopy (STEM-EDS) with an average nickel loading of ~ 0.7 atoms per Zr₆ node determined through inductively coupled plasma-atomic emission spectroscopy (ICP-AES) (Section S2, Figures S1, S2, S4, and S5; Tables S2 and S3).

Received: September 2, 2021 Published: November 24, 2021





The catalytic behavior of Ni/UiO-66 was probed by examining ethylene oligomerization after treating the material in $0.83~{\rm cm}^3~{\rm s}^{-1}$ of helium (Matheson, 99.997%) at 573 K for 4 h. The nascent Ni/UiO-66 is a precatalyst that activates on stream at various ethylene pressures ($106-2500~{\rm kPa}$) and in the absence of cocatalysts, as shown in Figure 1a. The catalyst



reaches a steady state at ethylene pressures ≤1000 kPa and, atypically for heterogeneous Ni-based ethylene oligomerization catalysts, maintains stable rates. We observe shorter induction periods for ethylene oligomerization as ethylene pressure is increased, which suggests that ethylene pressures impact the rate at which surface species necessary for attaining steady-state rates are formed.

The effect of ethylene pressure, shown in Figure 1b, was explored further by increasing the ethylene pressure on stream once the catalyst had reached steady state at 106 kPa, with the rate characteristics for 150–600 ks time on stream shown in Figure S9. Using a reference condition of 106 kPa ethylene pressure, increasing ethylene pressure to 657 kPa and lowering ethylene pressure back to 106 kPa ($\sim 0-150 \text{ ks}$; $\sim 600-750 \text{ ks}$) increases the rate of oligomerization by 5×. However, a step change in ethylene pressure from 106 kPa back to 657 kPa ($\sim 750-900 \text{ ks}$) reveals that the same intrinsic rate is observed at 657 kPa. After exposing the catalyst to 1000 kPa ethylene pressure ($\sim 900-1200 \text{ ks}$) and decreasing the ethylene pressure to 657 and 106 kPa ($\sim 1200-1500 \text{ ks}$), the intrinsic

rate of oligomerization at each condition increased by 50% from the reaction rates at \sim 600–900 ks. Remarkably, the catalyst is stable for 17 days on stream, which stands in marked contrast to other nickel-supported²¹ and framework-based²² MOFs and nickel-functionalized zeolites^{9–11,23} for oligomerization. We surmise the increase in reaction rates at the same ethylene partial pressures after subsequent exposure to higher ethylene pressures can be attributed either to a change in the nature of the active sites or to an increase in the number of active sites.

Enhancement in catalytic rates on stream by generation or alteration of active sites can be reasoned by plotting selectivities at isoconversion, as illustrated in methanol-to-hydrocarbons²⁴ and methane dehydroaromatization²⁵ catalysis. In Figure 1c, we present steady-state product selectivities at 106 kPa after exposing the catalyst to ethylene pressures of 657 and 1000 kPa with the flow rate of ethylene (0.25–1.5 cm³ s⁻¹ STP) regulated to maintain isoconversion. Product selectivities overlay at isoconversion, indicating that only one type of active site is relevant and formed during ethylene oligomerization by exposure to higher ethylene pressures.

Observations in Figure 1a,b present initiation periods that are shorter at higher ethylene pressures plausibly due to higher site densities induced in more facile stoichiometric reactions with ethylene at higher ethylene pressures. Thus, we employed NO titration experiments to enumerate the number of nickel active sites in situ during ethylene oligomerization, with the flow rates for butene, Ar, and NO shown in Figure 1d. An equimolar mixture of Ar and NO was introduced to the catalyst bed after steady-state time-on-stream rates were observed, and a decrease in butene flow rate was observed upon introduction of NO. The Ar flow achieves breakthrough while NO has a delayed breakthrough response attributed to the adsorption of NO on the nickel active sites that in turn impedes butene formation. The total number of active sites can be estimated by mathematical integration between the Ar and NO breakthrough curves, normalized by the amount of catalyst loaded (50–200 mg) at various ethylene pressures (110–1800 kPa) and is reported in Table 1. An ex situ NO titration on the

Table 1. Experimental Conditions and Ni Titrated for in Situ NO Titrations for Ethylene Oligomerization on Ni/UiO-66 at $473~\mathrm{K}$

ethylene pressure (kPa)	NO flow rate $(10^{-8} \text{ mol s}^{-1})$	Ni titrated $(\mu \text{mol } g_{\text{cat}}^{-1})$
110	3.48	4.1
111	3.48	5.5
200	2.09	13
500	3.48	15
500	3.48	16
500	3.48	24
1000	6.96	21
1000	13.9	23
1800	13.9	51

pristine UiO-66 MOF (Figure S19) is reported to demonstrate that NO binds to the nickel active site as opposed to the inactive MOF framework. The tabulated values illustrate that the number of active sites indeed increases with increasing ethylene pressures. At 1800 kPa, it appears only ~12% of the nickel sites are active for oligomerization from ~430 μ mol g_{cat}^{-1} calculated from ICP-AES (Table S3), assuming one NO

binds to one nickel atom to suppress the rate of oligomerization. Prior reports on Ni/NU-1000, a zirconium based MOF, ^{21,26,27} show isolated nickel atoms and clusters are supported on the MOF framework, and thus, we postulate that only some of the Ni species present are relevant for ethylene oligomerization.

On-stream generation of nickel sites with increasing ethylene pressures requires enumeration of active sites formed during reaction and then normalization of rates per mole of active nickel species to determine oligomerization reaction orders with respect to ethylene pressure. After accounting for the increase in the number of active sites formed upon exposure to high ethylene pressures, rates are first order in ethylene pressure as shown in Figure 2a, whereas rates appear second

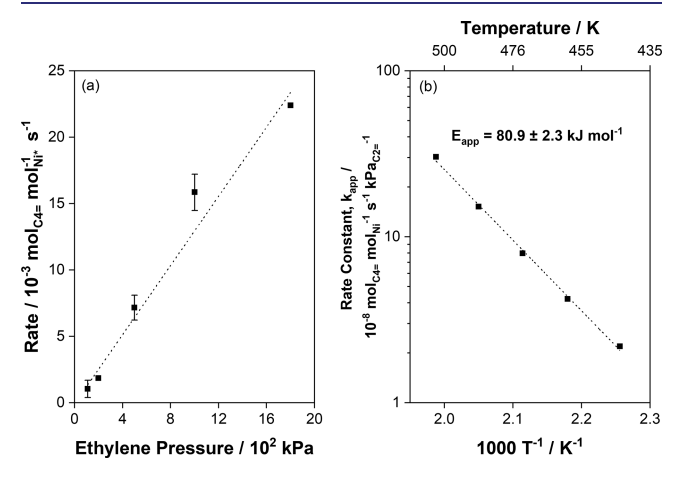


Figure 2. (a) Butene formation rate versus ethylene partial pressures (110-1800 kPa) at 473 K. (b) Arrhenius plot at 500 kPa on 40.0 mg Ni/UiO-66 and 0.83 cm³ s⁻¹ STP for ethylene oligomerization from 443 to 503 K.

order in ethylene pressure when active site densities are not enumerated (Figure S10). An Arrhenius plot, shown in Figure 2b, from temperatures of 443–503 K yields an apparent activation enthalpy of 80.9 ± 2.3 kJ mol⁻¹. We note that the number of active sites is unchanged with changing temperatures (Figure S11).

We report a mechanistic sequence for ethylene oligomerization to rationalize our observed induction periods and reaction kinetics utilizing DFT calculations on cluster models of Ni/UiO-66. The initiation mechanism 10,11,28 (A to H in Scheme 1) involves a series of stoichiometric reactions with the first step involving heterolytic activation of a C–H bond in ethylene to form a [Ni-vinyl] (C) and an acidic $[\mu_3\text{-OH}]^+$ complex, which is similar to initiation mechanisms proposed on Ni-containing zeolites where a proton from ethylene is abstracted to form a [Ni-vinyl-H] complex. $^{10,11,28-30}$ After the formation of C, another ethylene molecule is adsorbed (D) and inserts into the Ni-vinyl bond to form a [Ni-CH₂CH₂CH=CH₂] species (E). Species E undergoes β -hydride elimination to form butadiene bound to the active site (F), and a nickel hydride species (G) is formed upon subsequent desorption of butadiene. 10,11,28

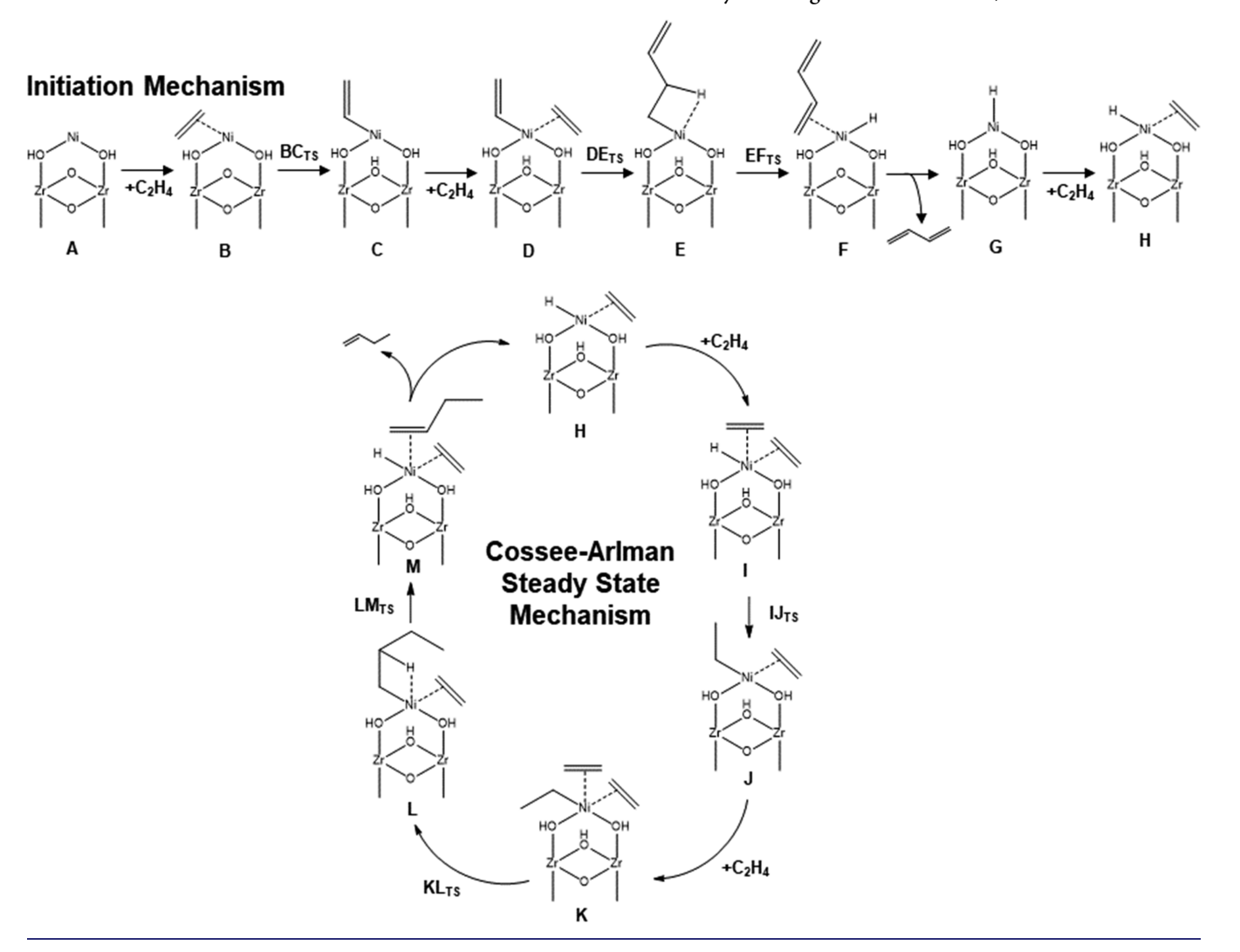
Steady-state oligomerization kinetics are proposed to follow the Cossee–Arlman mechanism, which typically initiates with formation of a nickel hydride species (**G** in Scheme 1 and **CA-1** in Scheme S1). ^{6–8,10,12–14,22,24,29,31} DFT calculations carried out using cluster models of Ni/UiO-66 result in near zero

apparent activation energies that are inconsistent with firstorder kinetics and activation energies observed experimentally (Table S8 and Figure S24). Hence, we employed ab initio thermodynamic analysis (see SI) to probe the active site composition under reaction conditions. Thermodynamic modeling suggests among candidate structures plausible at steady-state conditions (Scheme 1 and S1), a nickel-ethyl species (CA-3 in Scheme S1) requires the presence of an additional ethylene adsorbate for ethylene pressures greater than ~100 kPa (Figure 3). Thus, we employ a more representative model of the active site environment that accounts for physisorbed ethylene in the pores of the MOF at the experimental operating conditions (110-1800 kPa) in cluster model DFT calculations throughout the catalytic cycle. This model incorporates one extra adsorbed ethylene molecule to influence the reaction energetics and nature of the active site. A similar model on Ni-SSZ-24 with physisorbed ethylene molecules was able to replicate experimentally determined activation energies with DFT calculations. 11 Experimentally, catalytic stability for ethylene oligomerization on Ni-MCM-41 is reported at 1500 kPa and subambient temperatures, and this stability is ascribed to solvation by ethylene molecules. At lower ethylene pressures (<900 kPa), the intrapore liquid is absent in Ni-MCM-41 which alters the reaction pathway to promote oligomerization to form higher olefins and deactivate the catalyst. In the Ni/UiO-66 system reported herein, we observe catalytic stability at lower ethylene pressures (<1000 kPa) and elevated temperatures (443-503 K) to plausibly suggest physisorbed ethylene stabilizes nickel active site at our process conditions. 12 Furthermore, previous studies on homogeneous nickel catalysts have suggested that an additional olefin facilitates the formation of a five-coordinated transition state which in turn enables β -hydride elimination required to desorb the resultant oligomer and enable subsequent chain growth during oligomerization.³⁶ Along the same lines, we posit that solvation by ethylene facilitates olefin insertion into the Ni-C bond for chain growth. Coadsorbed ethylene prevents the formation of a stable, unreactive surface-bound intermediate (K) and destabilizes the kinetically relevant transition state for this step (KLTS) relative to a four coordinated nickel-ethyl-ethylene complex (J). 36,37 For these reasons, we postulate that structure H, a nickel hydride species with ethylene adsorbed on the active site, is relevant for the Cossee-Arlman mechanism operative in our system.

From **H**, another ethylene molecule is adsorbed to yield structure **I**. A migratory hydride insertion transforms species **I** to a nickel-ethyl species (**J**). From species **J**, another ethylene molecule is adsorbed (**K**) and inserts into the Ni–C bond to produce a nickel-butyl species (**L**). The nickel butyl species undergoes β -hydride elimination to produce 1-butene adsorbed on the surface (**M**) and regenerate the nickel hydride active site with ethylene adsorbed (**H**).

Enthalpy (red) and free energy (blue) diagrams for ethylene oligomerization on Ni/UiO-66 are presented for the initiation mechanism and the Cossee-Arlman mechanism in Figure S23 and Figure 4, respectively. We examined various spin states of Ni and report here the lowest energy spin state structures ($S^2 = 0$) with results from other spin states reported in the SI along with optimized reaction coordinates. The intrinsic free energy barrier for the C–H activation of the bound olefin (BC_{TS}) during the initiation mechanism is 141 kJ mol⁻¹ at 298 K and ambient pressure, which is consistent with the 153 kJ mol⁻¹ intrinsic free energy barrier calculated on Ni-AIM+NU-1000

Scheme 1. Initiation Mechanism and Cossee-Arlman Mechanism for Ethylene Oligomerization on Ni/UiO-66



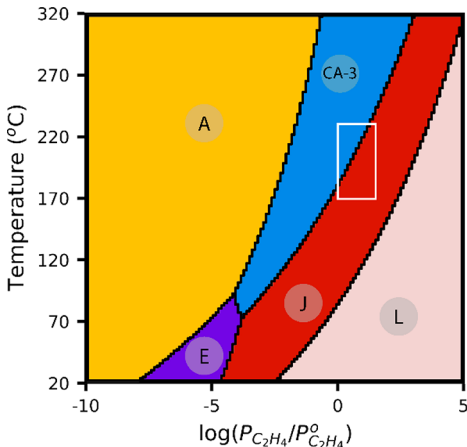


Figure 3. Phase diagram for the Ni/UiO-66 catalyst model calculated as a function of $P_{C_2H_4}$ (relative to standard pressure) and temperature at a constant 1,3-butadiene partial pressure of 0.05 Pa. Candidate structures were those utilized in Schemes 1 and S1; thermodynamically stable structures are those indicated in the phase diagram.

for C–H activation. ³¹ Olefin insertion into the Ni-vinyl bond (DE_{TS}) and the β -hydride elimination step (EF_{TS}) have intrinsic free energy barriers of 15 and 31 kJ mol⁻¹,

respectively. The free energy of adsorption of an ethylene molecule from G to H is -49 kJ mol $^{-1}$. From experiment, butadiene is observed at all ethylene pressures during the first 100 min on stream (Figure S14), which is consistent with the β -hydride elimination step (EF_{TS}) where butadiene is formed. Additionally, shorter induction periods and an increase in the number of active sites per gram catalyst are observed with increasing ethylene pressures (Figure 1 and Table 1), which is congruous with the stoichiometric formation of active sites dependent on ethylene pressure proposed in the initiation mechanism.

The steady-state Cossee—Arlman mechanism begins with species **H** followed by adsorption of an ethylene molecule (**I**), resulting in a free energy of adsorption of 17 kJ mol⁻¹. The migratory insertion of the hydride and adsorbed ethylene molecule (\mathbf{IJ}_{TS}) has a barrier of 22 kJ mol⁻¹. From species J, the free energy for adsorbing another ethylene molecule is 18 kJ mol⁻¹. The olefin insertion step (\mathbf{KL}_{TS}), the kinetically relevant step in the Cossee—Arlman mechanism, transpires with a free energy barrier of 80 kJ mol⁻¹. The β -hydride elimination step (\mathbf{LM}_{TS}) yields a free energy barrier of 48 kJ mol⁻¹. Calculated free energy barriers for the migratory insertion, olefin insertion, and β -hydride elimination step for ethylene oligomerization on a model of Ni/NU-1000, where physisorbed ethylene was not incorporated, are 15, 55, 48 kJ

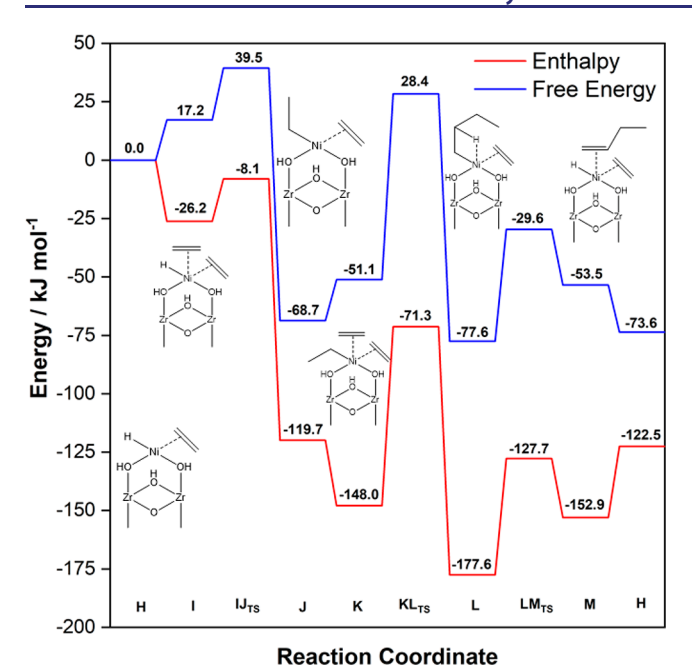


Figure 4. Enthalpy (red) and free energy (blue) diagram for the Cossee–Arlman mechanism with an extra ethylene molecule on the nickel for ethylene oligomerization on Ni/UiO-66 at 298 K and 101.3 kPa. All structures in the singlet spin state ($S^2 = 0$).

mol⁻¹, respectively, and are consistent with calculated free energy barriers on Ni/UiO-66 reported here. ^{4,31} With ethylene insertion into the Ni–C bond as the kinetically relevant step (KL_{TS}), experimentally determined first order kinetics with respect to ethylene (Figure 2a), and thermodynamic modeling results indicating additional adsorbed ethylene under reaction conditions (Figure 3), we propose J as the most abundant surface intermediate, which results in a calculated apparent activation enthalpy of 49 kJ mol⁻¹. This value is somewhat lower than the experimentally determined activation enthalpy of 81 kJ mol⁻¹. However, this mechanistic sequence and model are consistent with experimentally observed first-order kinetics in ethylene, induction periods that decrease with higher ethylene pressures, and stoichiometric events that form active sites on stream.

CONCLUSION

In summary, we report a nickel supported UiO-66 MOF that uniquely engenders active sites on stream and exhibits >15-day time-on-stream stability devoid of cocatalysts unprecedented in heterogeneous catalytic systems for ethylene oligomerization. Active site densities are enumerated in situ with NO titration experiments to disambiguate the effect of increased reaction rates with increasing ethylene pressures to appropriately determine first-order kinetics in ethylene pressure. A cluster model of Ni/UiO-66 that captures the effect of physisorbed ethylene is determined with ab initio thermodynamic modeling, and comparisons between experimental and computed apparent activation enthalpies validate the Cossee—Arlman mechanism for ethylene oligomerization on Ni/UiO-66 MOFs.

ASSOCIATED CONTENT

Supporting Information

The Supporting Information is available free of charge at https://pubs.acs.org/doi/10.1021/jacs.1c09320.

Experimental and computational details, materials characterization and synthesis, catalysis, density functional theory calculations, and atomic coordinates (PDF)

AUTHOR INFORMATION

Corresponding Authors

Laura Gagliardi — Department of Chemistry, Chemical Theory Center, and Supercomputing Institute, University of Minnesota—Twin Cities, Minneapolis, Minnesota 55455, United States; Department of Chemistry, The University of Chicago, Chicago, Illinois 60637, United States; orcid.org/0000-0001-5227-1396; Email: lgagliardi@uchicago.edu

Aditya Bhan — Department of Chemical Engineering and Materials Science, University of Minnesota—Twin Cities, Minneapolis, Minnesota 55455, United States; oorcid.org/0000-0002-6069-7626; Email: abhan@umn.edu

Authors

Benjamin Yeh – Department of Chemical Engineering and Materials Science, University of Minnesota–Twin Cities, Minneapolis, Minnesota 55455, United States

Stephen P. Vicchio – Department of Chemical and Biomolecular Engineering, Clemson University, Clemson, South Carolina 29634-0909, United States

Saumil Chheda — Department of Chemical Engineering and Materials Science, University of Minnesota—Twin Cities, Minneapolis, Minnesota 55455, United States; Department of Chemistry, Chemical Theory Center, and Supercomputing Institute, University of Minnesota—Twin Cities, Minneapolis, Minnesota 55455, United States

Jian Zheng – Institute for Integrated Catalysis, Pacific Northwest National Laboratory, Richland, Washington 99352, United States

Julian Schmid — Institute for Integrated Catalysis, Pacific Northwest National Laboratory, Richland, Washington 99352, United States

Laura Löbbert – Department of Chemistry and Catalysis Research Center, Technical University of Munich, 85748 Garching, Germany

Ricardo Bermejo-Deval – Department of Chemistry and Catalysis Research Center, Technical University of Munich, 85748 Garching, Germany

Oliver Y. Gutiérrez – Institute for Integrated Catalysis, Pacific Northwest National Laboratory, Richland, Washington 99352, United States; Orcid.org/0000-0001-9163-4786

Johannes A. Lercher — Institute for Integrated Catalysis,
Pacific Northwest National Laboratory, Richland,
Washington 99352, United States; Department of Chemistry
and Catalysis Research Center, Technical University of
Munich, 85748 Garching, Germany; orcid.org/00000002-2495-1404

Connie C. Lu — Department of Chemistry, Chemical Theory Center, and Supercomputing Institute, University of Minnesota—Twin Cities, Minneapolis, Minnesota 55455, United States; orcid.org/0000-0002-5162-9250

Matthew Neurock – Department of Chemical Engineering and Materials Science, University of Minnesota–Twin Cities, Minneapolis, Minnesota 55455, United States

Rachel B. Getman – Department of Chemical and Biomolecular Engineering, Clemson University, Clemson,

South Carolina 29634-0909, United States; o orcid.org/0000-0003-0755-0534

Complete contact information is available at: https://pubs.acs.org/10.1021/jacs.1c09320

Notes

The authors declare no competing financial interest.

ACKNOWLEDGMENTS

This work was supported by the Inorganometallic Catalyst Design Center, an Energy Frontier Research Center funded by the US Department of Energy (DOE), Office of Science, Basic Energy Sciences (BES) (DE-SC0012702). Benjamin Yeh acknowledges the National Science Foundation for a graduate research fellowship and a departmental scholarship funded by 3M. The authors acknowledge the Minnesota Supercomputing Institute (MSI) at the University of Minnesota for providing computational resources. PXRD and STEM-EDS were carried out in the Characterization Facility, University of Minnesota, which receives partial support from the National Science Foundation (NSF) through the MRSEC program, with help from Xinyu Li and Rebecca Combs, respectively. Our research used resources of the Advanced Photon Source, a DOE-Office of Science user facility operated by Argonne National Laboratory and was supported by DOE under Contract No. DE-AC02-06CH11357 and the Canadian Light Source and its funding partners. Part of this work was also performed at Stanford Synchrotron Radiation Lightsource (SSRL) of SLAC National Accelerator Laboratory by Co-ACCESS, supported by the U.S. Department of Energy, Office of Basic Energy Sciences, Chemical Sciences, Geosciences, and Biosciences Division. X-ray adsorption spectra were taken with the help of Dr. Mahalingam Balasubramanian and Dr. Adam Hoffman. We thank Dr. Brandon Foley, Dr. Jacob Miller, Dr. Matthew Simons, Zhichen Shi, and Neil Razdan for helpful technical discussions.

REFERENCES

- (1) Mol, J. C. Industrial Applications of Olefin Metathesis. *J. Mol. Catal. A: Chem.* **2004**, 213 (1), 39–45.
- (2) Keim, W. Oligomerization of Ethylene to α -Olefins: Discovery and Development of the Shell Higher Olefin Process (SHOP). *Angew. Chem., Int. Ed.* **2013**, 52 (48), 12492–12496.
- (3) Forestière, A.; Olivier-Bourbigou, H.; Saussine, L. Oligomérisation Des Mono-Oléfines Par Des Catalyseurs Homogènes. *Oil Gas Sci. Technol.* **2009**, 64 (6), 649–667.
- (4) Ye, J.; Gagliardi, L.; Cramer, C. J.; Truhlar, D. G. Computational Screening of MOF-Supported Transition Metal Catalysts for Activity and Selectivity in Ethylene Dimerization. *J. Catal.* **2018**, *360*, 160–167
- (5) Metzger, E. D.; Brozek, C. K.; Comito, R. J.; Dinca, M. Selective Dimerization of Ethylene to 1-Butene with a Porous Catalyst. *ACS Cent. Sci.* **2016**, 2 (3), 148–153.
- (6) Comito, R. J.; Metzger, E. D.; Wu, Z.; Zhang, G.; Hendon, C. H.; Miller, J. T.; Dincă, M. Selective Dimerization of Propylene with Ni-MFU-4l. *Organometallics* **2017**, *36* (9), 1681–1683.
- (7) Metzger, E. D.; Comito, R. J.; Hendon, C. H.; Dincă, M. Mechanism of Single-Site Molecule-like Catalytic Ethylene Dimerization in Ni-MFU-4l. *J. Am. Chem. Soc.* **2017**, *139* (2), 757–762.
- (8) Skupińska, J. Oligomerization of α -Olefins to Higher Oligomers. *Chem. Rev.* **1991**, *91* (4), 613–648.
- (9) Ehrmaier, A.; Liu, Y.; Peitz, S.; Jentys, A.; Chin, Y. H. C.; Sanchez-Sanchez, M.; Bermejo-Deval, R.; Lercher, J. Dimerization of Linear Butenes on Zeolite-Supported Ni 2+. *ACS Catal.* **2019**, 9 (1), 315–324.

- (10) Henry, R.; Komurcu, M.; Ganjkhanlou, Y.; Brogaard, R. Y.; Lu, L.; Jens, K.-J.; Berlier, G.; Olsbye, U. Ethene Oligomerization on Nickel Microporous and Mesoporous-Supported Catalysts: Investigation of the Active Sites. *Catal. Today* **2018**, 299, 154–163.
- (11) Brogaard, R. Y.; Kømurcu, M.; Dyballa, M. M.; Botan, A.; Van Speybroeck, V.; Olsbye, U.; De Wispelaere, K. Ethene Dimerization on Zeolite-Hosted Ni Ions: Reversible Mobilization of the Active Site. *ACS Catal.* **2019**, *9* (6), 5645–5650.
- (12) Agirrezabal-Telleria, I.; Iglesia, E. Stabilization of Active, Selective, and Regenerable Ni-Based Dimerization Catalysts by Condensation of Ethene Withinordered Mesopores. *J. Catal.* **2017**, 352, 505–514.
- (13) Cavka, J. H.; Jakobsen, S.; Olsbye, U.; Guillou, N.; Lamberti, C.; Bordiga, S.; Lillerud, K. P. A New Zirconium Inorganic Building Brick Forming Metal Organic Frameworks with Exceptional Stability. *J. Am. Chem. Soc.* **2008**, *130* (42), 13850–13851.
- (14) Shearer, G. C.; Chavan, S.; Ethiraj, J.; Vitillo, J. G.; Svelle, S.; Olsbye, U.; Lamberti, C.; Bordiga, S.; Lillerud, K. P. Tuned to Perfection: Ironing out the Defects in Metal-Organic Framework UiO-66. Chem. Mater. 2014, 26 (14), 4068–4071.
- (15) Biswas, S.; Van Der Voort, P. A General Strategy for the Synthesis of Functionalised UiO-66 Frameworks: Characterisation, Stability and CO2 Adsorption Properties. *Eur. J. Inorg. Chem.* **2013**, 12, 2154–2160.
- (16) Trickett, C. A.; Gagnon, K. J.; Lee, S.; Gándara, F.; Bürgi, H. B.; Yaghi, O. M. Definitive Molecular Level Characterization of Defects in UiO-66 Crystals. *Angew. Chem., Int. Ed.* **2015**, *54* (38), 11162–11167.
- (17) Katz, M. J.; Brown, Z. J.; Colón, Y. J.; Siu, P. W.; Scheidt, K. A.; Snurr, R. Q.; Hupp, J. T.; Farha, O. K. A Facile Synthesis of UiO-66, UiO-67 and Their Derivatives. *Chem. Commun.* **2013**, 49 (82), 9449–9451.
- (18) Nguyen, H. G. T.; Schweitzer, N. M.; Chang, C. Y.; Drake, T. L.; So, M. C.; Stair, P. C.; Farha, O. K.; Hupp, J. T.; Nguyen, S. T. Vanadium-Node-Functionalized UiO-66: A Thermally Stable MOF-Supported Catalyst for the Gas-Phase Oxidative Dehydrogenation of Cyclohexene. ACS Catal. 2014, 4 (8), 2496–2500.
- (19) Abdel-Mageed, A. M.; Rungtaweevoranit, B.; Parlinska-Wojtan, M.; Pei, X.; Yaghi, O. M.; Behm, R. J. Highly Active and Stable Single-Atom Cu Catalysts Supported by a Metal-Organic Framework. *J. Am. Chem. Soc.* **2019**, *141* (13), 5201–5210.
- (20) Goetjen, T. A.; Zhang, X.; Liu, J.; Hupp, J. T.; Farha, O. K. Metal-Organic Framework Supported Single Site Chromium(III) Catalyst for Ethylene Oligomerization at Low Pressure and Temperature. ACS Sustainable Chem. Eng. 2019, 7 (2), 2553–2557.
- (21) Liu, J.; Ye, J.; Li, Z.; Otake, K. I.; Liao, Y.; Peters, A. W.; Noh, H.; Truhlar, D. G.; Gagliardi, L.; Cramer, C. J.; et al. Beyond the Active Site: Tuning the Activity and Selectivity of a Metal-Organic Framework-Supported Ni Catalyst for Ethylene Dimerization. *J. Am. Chem. Soc.* **2018**, *140* (36), 11174–11178.
- (22) Mlinar, A. N.; Keitz, B. K.; Gygi, D.; Bloch, E. D.; Long, J. R.; Bell, A. T. Selective Propene Oligomerization with Nickel(II)-Based Metal-Organic Frameworks. *ACS Catal.* **2014**, *4* (3), 717–721.
- (23) Joshi, R.; Zhang, G.; Miller, J. T.; Gounder, R. Evidence for the Coordination-Insertion Mechanism of Ethene Dimerization at Nickel Cations Exchanged onto Beta Molecular Sieves. *ACS Catal.* **2018**, 8 (12), 11407–11422.
- (24) Foley, B. L.; Johnson, B. A.; Bhan, A. A Method for Assessing Catalyst Deactivation: A Case Study on Methanol-to-Hydrocarbons Conversion. *ACS Catal.* **2019**, *9* (8), 7065–7072.
- (25) Razdan, N. K.; Kumar, A.; Foley, B. L.; Bhan, A. Influence of Ethylene and Acetylene on the Rate and Reversibility of Methane Dehydroaromatization on Mo/H-ZSM-5 Catalysts. *J. Catal.* **2020**, 381, 261–270.
- (26) Ye, J.; Gagliardi, L.; Cramer, C. J.; Truhlar, D. G. Single Ni Atoms and Ni4 Clusters Have Similar Catalytic Activity for Ethylene Dimerization. *J. Catal.* **2017**, *354*, 278–286.
- (27) Platero-Prats, A. E.; League, A. B.; Bernales, V.; Ye, J.; Gallington, L. C.; Vjunov, A.; Schweitzer, N. M.; Li, Z.; Zheng, J.;

- Mehdi, B. L.; et al. Bridging Zirconia Nodes within a Metal-Organic Framework via Catalytic Ni-Hydroxo Clusters to Form Heterobimetallic Nanowires. *J. Am. Chem. Soc.* **2017**, *139* (30), 10410–10418.
- (28) Brogaard, R. Y.; Olsbye, U. Ethene Oligomerization in Ni-Containing Zeolites: Theoretical Discrimination of Reaction Mechanisms. ACS Catal. 2016, 6 (2), 1205–1214.
- (29) Moussa, S.; Concepción, P.; Arribas, M. A.; Martínez, A. Nature of Active Nickel Sites and Initiation Mechanism for Ethylene Oligomerization on Heterogeneous Ni-Beta Catalysts. *ACS Catal.* **2018**, *8* (5), 3903–3912.
- (30) Planas, N.; Mondloch, J. E.; Tussupbayev, S.; Borycz, J.; Gagliardi, L.; Hupp, J. T.; Farha, O. K.; Cramer, C. J. Defining the Proton Topology of the Zr6-Based Metal-Organic Framework NU-1000. J. Phys. Chem. Lett. 2014, 5 (21), 3716–3723.
- (31) Bernales, V.; League, A. B.; Li, Z.; Schweitzer, N. M.; Peters, A. W.; Carlson, R. K.; Hupp, J. T.; Cramer, C. J.; Farha, O. K.; Gagliardi, L. Computationally Guided Discovery of a Catalytic Cobalt-Decorated Metal-Organic Framework for Ethylene Dimerization. *J. Phys. Chem. C* 2016, 120 (41), 23576–23583.
- (32) Grundner, S.; Markovits, M. A. C.; Li, G.; Tromp, M.; Pidko, E. A.; Hensen, E. J. M.; Jentys, A.; Sanchez-Sanchez, M.; Lercher, J. A. Single-Site Trinuclear Copper Oxygen Clusters in Mordenite for Selective Conversion of Methane to Methanol. *Nat. Commun.* **2015**, *6* (May), 1–9.
- (33) Paolucci, C.; Parekh, A. A.; Khurana, I.; Di Iorio, J. R.; Li, H.; Albarracin Caballero, J. D.; Shih, A. J.; Anggara, T.; Delgass, W. N.; Miller, J. T.; et al. Catalysis in a Cage: Condition-Dependent Speciation and Dynamics of Exchanged Cu Cations in Ssz-13 Zeolites. *J. Am. Chem. Soc.* **2016**, *138* (18), 6028–6048.
- (34) Getman, R. B.; Xu, Y.; Schneider, W. F. Thermodynamics of Environment-Dependent Oxygen Chemisorption on Pt(111). *J. Phys. Chem. C* **2008**, *112* (26), 9559–9572.
- (35) Soon, A.; Todorova, M.; Delley, B.; Stampfl, C. Surface Oxides of the Oxygen Copper System Precursors to the Bulk Oxide Phase. *Surf. Sci.* **2007**, *601*, 5809–5813.
- (36) Ittel, S. D.; Johnson, L. K.; Brookhart, M. Late-Metal Catalysts for Ethylene Homo- and Copolymerization. *Chem. Rev.* **2000**, *100* (4), 1169–1203.
- (37) Musaev, D. G.; Morokuma, K. Theoretical Studies of the Mechanism of Ethylene Polymerization Reaction Catalyzed by Diimine-M(II) (M = Ni, Pd and Pt) and Ti- and Zr-Chelating Alkoxides. *Top. Catal.* **1999**, 7 (1–4), 107–123.